Combustion and Flame 227 (2021) 65–78

Contents lists available at ScienceDirect

Combustion and Flame

journal homepage: www.elsevier.com/locate/combustflame

The effect of turbulence on mass transfer in solid fuel combustion: RANS model

Ewa Karchniwy[a,b,*], Nils Erland L. Haugen[c], Adam Klimanek[a], Øyvind Langørgen[c], Sławomir Sładek[a]

[a] Department of Thermal Technology, Silesian University of Technology, Konarskiego 22, Gliwice 44-100, Poland
[b] Department of Energy and Process Engineering, Norwegian University of Science and Technology, Kolbjørn Hejes vei 1B, Trondheim NO-7491, Norway
[c] SINTEF Energi A.S., Sem Saelands vei 11, Trondheim 7034, Norway

ARTICLE INFO

Article history:
Received 20 August 2020
Revised 14 December 2020
Accepted 28 December 2020

Keywords:
Combustion kinetics
Combustion rates
Char oxidation
Diffusion regime

ABSTRACT

In this paper, a kinetic-diffusion surface combustion model is examined. The model is modified such that two effects of turbulence are included: 1) enhancement of the mass transfer due to relative velocity between particles and fluid and 2) reduction of the mass transfer due to turbulence-induced particle clustering. Details of the implementation are discussed and the influence of parameters such as air-fuel ratio, particle number density, particle diameter, turbulence intensity and characteristic length scales are studied theoretically. A simplified numerical model of a combustion chamber is created to explore the effects of the combustion model predictions. Finally, the model is incorporated into simulations of an industrial-scale boiler to investigate the effect of turbulence on the net surface reaction rate in a real system. The study shows that although on average this effect is rather minor, there exist regions in which the carbon conversion rate is either decreased or increased by turbulence.

1. Introduction

Modelling of solid fuels combustion and gasification requires taking into account several important processes occurring during fuel conversion. A solid fuel particle injected into a hot environment is first heated up and dried. In the next stage devolatilization starts, which is a complex decomposition process associated with the release of multiple gaseous products. During the last stage of conversion, the remaining char is converted through reactions with the surrounding gas. In reality, a distinct separation between the processes can typically not be distinguished, and the drying and devolatilization, as well as devolatilization and char surface reactions overlap [1,2], in particular for large particles. The devolatilization is much faster than the char conversion, especially in gasification systems, where slow endothermic reactions are responsible for the char conversion rate. Many parameters affect the devolatilization process leading to different volatile compositions, total yield and reaction rate. A range of models have previously been developed, differing considerably by their complexity and accuracy, see [2–5] for more detailed information on the process and its modelling.

The final stage of fuel conversion, i.e. the char conversion process, is affected by: the diffusion of reactants from the surrounding fluid to the particle surface, diffusion within particle pores, heterogeneous reactions at external and internal particle surfaces (including reactant gas adsorption and desorption), evolution of the char internal structure of pores, ash inhibition and thermal annealing [6]. Several approaches to char conversion modeling have been proposed in the literature. Among the most commonly used is the kinetic-diffusion surface reaction rate model [7,8] according to which the overall reaction rate can be influenced both by the reaction kinetics and the reactant diffusion. This model uses global kinetics and is computationally very efficient but it does not explicitly account for processes such as evolution of the char intrinsic surface area and pore diffusion, nor does it consider changes in particle diameter and density, variations in the particle reactivity [9], thermal deactivation or ash inhibition. A much more detailed approach that includes all of the above-mentioned processes is the Carbon Burnout Kinetics (CBK) model proposed by Hurt et al. [10] and further extended to oxidation and gasification at elevated pressure by Niksa et al. [11] and Liu & Niksa [12]. The CBK model was developed specifically to correctly predict char burnout and is able to capture a lower reactivity of chars at the final stage of

* Corresponding author at: Department of Thermal Technology, Silesian University of Technology, Konarskiego 22, Gliwice 44-100, Poland.
E-mail address: ewa.karchniwy@polsl.pl (E. Karchniwy).

https://doi.org/10.1016/j.combustflame.2020.12.040

conversion. However, the computational expense makes the model impractical to use in large-scale simulations [6]. More recently, groups at Stanford University and SINTEF have developed a model similar to the CBK model [13–15]. This model has a more accurate description of the size and density evolution of the char, together with a detailed intrinsic reaction mechanism. Annealing is, however, not included in this model.

Solid fuel combustion in industrial-scale facilities most often occurs under turbulent conditions. From the processes involved in char conversion mentioned above, turbulence primarily affects the efficiency of the reactant transport towards the particle surface. This effect of turbulence has been a subject of several recent studies [16–19]. Using Direct Numerical Simulations (DNS) and a simplified case in which a passive scalar (reactant) was consumed isothermally, the authors of [16,17] showed that turbulence might have two effects that counteract each other. Krüger et al. [16] demonstrated that the overall conversion rate can be reduced if the turbulent flow promotes particle clustering. This is related to the rapid oxidizer depletion due to increased concentration of particles in the clusters. These studies were extended by Haugen et al. [17] who showed that, in addition to particle clustering, turbulence can also increase the rate of heterogeneous reactions through velocity fluctuations that intensify the reactant transfer towards the particle surface. Furthermore, Haugen et al. [17] formulated a model that modifies the mass transfer coefficient to account for the two effects of turbulence and verified the model against their DNS results. These investigations were further extended to more realistic, non-isothermal conditions [18] and systems of polydisperse particles [19].

In the current study, we focus on the effects of turbulence on the mass transfer from the bulk gas to the particle surface. We discuss the model developed by Haugen et al. [17] and apply it to realistic combustion cases by utilizing the Reynolds Averaged Navier-Stokes (RANS) approach. Both main effects are considered: the enhancement of mass transfer through velocity fluctuations and the mass transfer rate reduction due to turbulence-induced particle clustering. We study the parameters affecting the process and show how the two effects of turbulence influence the char conversion in a jet of particles and in an industrial-scale boiler.

2. Theory

The reactant consumption rate of a fuel particle can be defined as the normalized quantity relating the rate of change of particle mass, m_p, and its initial mass, $m_{p,0}$,

$$\Theta = -\frac{1}{m_{p,0}}\frac{dm_p}{dt} \tag{1}$$

In order to reduce complexity of the analysis we limit our discussion to the context of char burnout. We apply a simple kinetic-diffusion model, with apparent rate kinetics. It should be stressed, however, that the analysis can be easily extended to more detailed models.

2.1. Kinetic-diffusion model

One of the most frequently used approaches in CFD modelling of solid fuels combustion and gasification is to apply the kinetic-diffusion model, given by

$$\Theta = \frac{\pi d_p^2 p_{ox}}{m_{p0}}\frac{1}{1/R_{dif} + 1/R_{kin}}, \tag{2}$$

where d_p is the particle diameter, p_{ox} is the partial pressure of oxidizer, R_{dif} is the reaction rate due to diffusion defined as

$$R_{dif} = \frac{C}{d_p}\left(\frac{T+T_p}{2}\right)^{3/4} \tag{3}$$

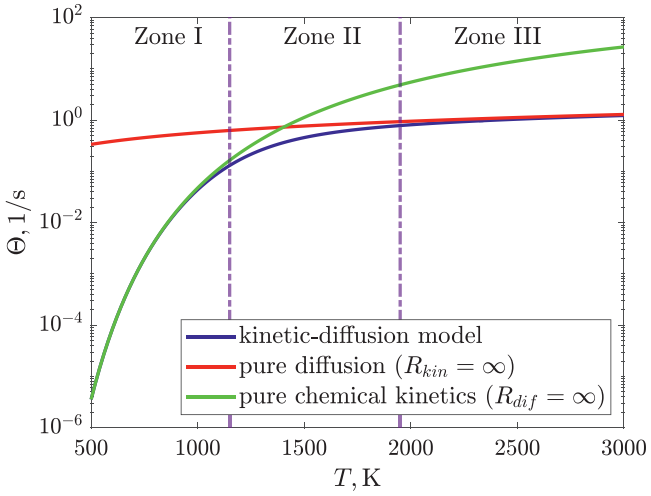

Fig. 1. The kinetic-diffusion model for $T_p = T$, $\rho_p = 800$ kg/m^3, $d_p = 500$ μm, $A = 0.002$ s/m, $E = 79$ kJ/mol, $C = 5 \cdot 10^{-12}$ sK$^{-3/4}$.

and R_{kin} is the kinetic reaction rate, which is often written in the Arrhenius form

$$R_{kin} = A\exp\left(-\frac{E}{RT_p}\right). \tag{4}$$

In the above equations C is a constant, T_p and T are the temperatures of the particle and of the gas surrounding the particle, respectively, A is the pre-exponential factor, E is the activation energy, and R is the universal gas constant. The kinetic rate R_{kin} is the apparent rate, therefore the intrinsic reactivity and pore diffusion is already accounted for in parameters A and E. The model can be extended to account for these effects explicitly, see for example [20–22]. The kinetic-diffusion model, as given in Eq. (2), was derived with the assumption that the reaction is first order with respect to the oxidizer ox, see Smith [20] for details. In Fig. 1 the prediction of the kinetic-diffusion model is plotted as a function of temperature for a given condition. The effects of pure chemical kinetics ($R_{dif} = \infty$) and pure diffusion ($R_{kin} = \infty$) are also shown. As can be seen, the chemical reactions are slow at low temperatures and limits the overall reaction rate (Zone I). At high temperatures, the chemical reactions are fast, and the overall reaction rate is limited by the transport of oxidizer to the particle surface (Zone III). Between zones I and III, an intermediate temperature range exists (Zone II) in which both chemical kinetics and diffusion are important in determining the overall reaction rate.

2.2. The effect of mean gas-particle velocity difference

The constant C entering Eq. (3) incorporates all the effects responsible for mass transfer to the particle surface, i.e. the stoichiometry of the reaction, diffusion to the particle surface and the effect of convection. Chen et al. [23] proposed that for the ith reaction

$$C_i = s_i\frac{M_C}{M_i}\frac{\overline{M}}{RT_0^{7/4}}\frac{p_0}{p}\mathrm{Sh}D_{i,0}. \tag{5}$$

This is an extension of a formula derived by Baum et al. [7] for a single oxidation reaction. Here, s_i is the ratio of the stoichiometric coefficients of carbon and reactant (e.g. $s_i = 1$ for $C + O_2 \rightarrow CO_2$; $s_i = 2$ for $2C + O_2 \rightarrow 2CO$), M_C and M_i are the molecular weights of carbon and the reactant of reaction i, respectively, $\overline{M}$ is the mean molecular weight of the gas in the particle boundary layer, Sh is the Sherwood number, D_i is the diffusion coefficient of the gaseous

reactant of reaction i, p is pressure and subscript 0 denotes the reference state. Assuming that the particles can be treated as spheres, the Sherwood number can be determined from the Ranz-Marshall formula [24]

$$\mathrm{Sh} = 2.0 + 0.6\mathrm{Re}_p^{1/2}\mathrm{Sc}^{1/3}, \tag{6}$$

where $\mathrm{Sc} = \nu/D$ is the Schmidt number, and Re_p is the particle Reynolds number defined as

$$\mathrm{Re}_p = \frac{|u_p - u| d_p}{\nu}, \tag{7}$$

where u is the mean gas velocity, u_p is the particle velocity and ν is the kinematic viscosity. It has frequently been argued [20], that for fine pulverized fuel particles the relative particle-gas velocity is small, and thus $\mathrm{Re_p} \to 0$ and $\mathrm{Sh} \to 2$. However, the particle Reynolds numbers can become higher for pressurized systems such as entrained-flow gasification reactors [25]. Also, for larger particles, characterized by larger Stokes numbers, the effect can become important as well.

In modelling of dilute, particulate flows, the effect of turbulence on particle dispersion is often included. One of the most frequently used approaches is to apply a stochastic tracking method. In such a case the particle trajectory is computed based on the instantaneous fluid velocity, which is a sum of the mean fluid velocity and its fluctuating component,

$$u' = \zeta\sqrt{2k/3}, \tag{8}$$

where ζ is a normally distributed random number and k is the turbulent kinetic energy. Even though this method may produce realistic particle dispersion, it gives rise to unphysically large relative velocity differences between particle and fluid. Remember that even tracer particles will experience this unphysical relative velocity, even though they in reality will always follow the fluid in which they are embedded. This is because it is the unresolved turbulent eddies that transport the particles. In turn, such an exagerated relative velocity gives too large Sherwood number and hence too high transport rate of mass between fluid and particle. Therefore, in the following, we use a constant value of the Sherwood number when calculating C from Eq. (5), and include the effect of turbulence by applying a correction factor $\tilde{\alpha}$, as will be explained below.

2.3. The effect of turbulence and particle clustering

In practical systems the burning particle is exposed to rapid gas velocity fluctuations occurring due to turbulence. The turbulent motion can be responsible for considerable increase of oxidizer transport to the particle surface due to the induced velocity difference between the particle and the surrounding fluid, as discussed in the former section. However, the particles can also form clusters due to turbulence, which can lead to local oxidizer depletion and reduction of the reaction rate. These effects were studied by Direct Numerical Simulation in [16–19] and the following model was formulated for the turbulence correction factor

$$\tilde{\alpha} = \frac{\mathrm{Sh}_{mod}}{2} = \frac{\overline{\mathrm{Sh}}}{2}\underbrace{\frac{B}{B + \mathrm{DaSt}/2}}_{=\alpha_{\mathrm{cluster}}} \tag{9}$$

where $\frac{1}{2}\overline{\mathrm{Sh}}$ is the part corresponding to the effect of the relative velocity between the particles and the fluid, while $\alpha_{\mathrm{cluster}}$ is the part that corresponds to clustering. The model parameter B was shown by Haugen et al. [17] to vary with Stokes number as

$$B = 0.08 + \mathrm{St}/3. \tag{10}$$

Apart from the average Sherwood number, $\overline{\mathrm{Sh}}$, two dimensionless numbers enter Eq. (9), namely the Stokes number (St) and the Damköhler number (Da). They are defined as

$$\mathrm{St} = \tau_p/\tau_L, \tag{11}$$

$$\mathrm{Da} = \tau_L/\tau_c, \tag{12}$$

where τ_p is the particle response time, τ_L is the integral time scale of turbulence and τ_c is the chemical time scale, related to the combustion time. The particle response time is defined by the Stokes time

$$\tau_p = \frac{\rho_p d_p^2}{18\rho\nu}, \tag{13}$$

where ρ_p is the particle (material) density and ρ is the gas density. The integral time scale can be written as

$$\tau_L = \frac{2}{3}\frac{k}{\varepsilon} \tag{14}$$

and the chemical time scale is defined as

$$1/\tau_c = n_p A_p \frac{\overline{\mathrm{Sh}}}{D} d_p, \tag{15}$$

where $A_p = \pi d_p^2$ is the particle external surface area and

$$n_p = \frac{6\rho_s}{\rho_p \pi d_p^3} \tag{16}$$

is the particle number density with ρ_s being the solids density in the mixture. Please note that ρ_p is the material (or apparent) density of the particle, which is very different from the solid density in the mixture, ρ_s. For example, the solid density of char in air at 1000 K and stoichiometric conditions is around 0.03 kg/m^3. This corresponds to nearly one hundred 100 µm-sized char particles per cubic centimeter for char particles with an apparent density of 600 kg/m^3.

In the following, the physical reasoning on which Eq. (9) was derived will be described. If the lifetime of a particle cluster ($\tau_{cluster}$) is short relative to the chemical time scale (τ_c), the reactant concentration can be assumed to be uniform across the cluster and equal to the concentration outside the cluster. In this case, the relevant reactant consumption rate is given by Eq. (15), which is valid for homogeneous distributions of particles and reactant. For clusters with long lifetimes compared to the chemical time scale, the reactant concentration inside the cluster is reduced. This means that the overall consumption rate becomes dependent on cluster characteristics, such as cluster dimension and particle number density. The resulting reactant consumption rate (r) is therefore limited both by the rate due to Eq. (15) ($r_{uniform} = 1/\tau_c$) and the cluster-characteristic rate ($r_{cluster} = 1/\tau_{cluster}$). This means that the reactant consumption rate, which equals the mass transfer rate, can be written as:

$$r = \frac{r_{uniform} r_{cluster}}{r_{uniform} + r_{cluster}}. \tag{17}$$

Therefore, when the above formulation is normalized using the reactant consumption rate from Eq. (15) with $\overline{\mathrm{Sh}} = 2$, denoted as $r_{uniform,\overline{\mathrm{Sh}}=2}$, one obtains a factor by which the mass transfer rate is altered relative to the rate typically used in RANS simulations:

$$\tilde{\alpha} = \left(\frac{r_{uniform} r_{cluster}}{r_{uniform} + r_{cluster}}\right) / r_{uniform,\overline{\mathrm{Sh}}=2}. \tag{18}$$

Using Eqs. (12) and (15), and after some rearranging, Eq. (9) can be recovered with $B = r_{cluster}\tau_L \mathrm{St}/2 = r_{cluster}\tau_p/2$. Since $r_{cluster}$ is unknown, an approximate expression for the parameter B was found using DNS (see Eq. (10)). The details on the fitting procedure are given in [17].

Previous studies [16,17] showed that the intensified transport of oxidizer towards the particle surface is the dominating effect of

turbulence at relatively low Da. However, as the Damköhler number gets larger, the impeded reactant transport associated with the particle clustering becomes the major phenomenon controlling the overall surface reaction rate. It was also found that the effect of clustering is strongest when the Stokes number is of the order of unity. The reason for that is that such conditions (i.e. similar magnitudes of particle and flow time scales) are the most conducive to the formation of relatively long-lived clusters. (It is well known that particle clusters at the Kolmogorov scale, which are due to particles with Kolmogorov based Stokes numbers around unity, are the strongest and sharpest, but these clusters typically have too short lifetimes to have any relevance for the reactant transport.)

The Sherwood number $\overline{\mathrm{Sh}}$ entering Eq. (9) can still be determined from Eq. (6), however, the particle Reynolds number should now be calculated as

$$\mathrm{Re}_p = \frac{u_{rel} d_p}{\nu} \tag{19}$$

such that the effect of turbulent velocity fluctuations is taken into account through the relative velocity, u_{rel}. Based on physical arguments, Haugen et al. [17] proposed the following expression for the average relative velocity difference caused by the turbulence:

$$u_{rel} = \beta u_{rms} \sqrt{\frac{\mathrm{St} k_L^{-2/3} - k_\eta^{-2/3}}{k_L^{-2/3} - k_\eta^{-2/3}}}, \tag{20}$$

where $\beta = 0.41$ is a model constant, k_L and k_η are the integral and Kolmogorov scale wavenumbers, respectively. The wave numbers can be linked to the turbulent kinetic energy k, its dissipation rate ε, and kinematic viscosity ν as

$$k_L = 2\pi \varepsilon \left(\frac{3}{2k}\right)^{3/2} \tag{21}$$

$$k_\eta = 2\pi \left(\frac{\varepsilon}{\nu^3}\right)^{1/4}. \tag{22}$$

The main assumption behind Eq. (20) is that the relative velocity is induced only by those turbulent eddies that have turnover times, τ_{eddy}, that are shorter than the particle response time, τ_p. In this way, the relative velocity is proportional to the square root of the kinetic energy ($E(\kappa)$) of the corresponding eddies, such that:

$$u_{rel} \sim \left(\int_{k_\eta}^{k_{eddy}} E(\kappa) dk\right)^{1/2} \sim \left(\int_{k_\eta}^{k_{eddy}} \varepsilon^{2/3} \kappa^{-5/3} dk\right)^{1/2} \tag{23}$$

where $k_{eddy} = 2\pi/\tau_{eddy} u_{eddy}$. Furthermore, Kolmogorov scaling for the inertial sub-range was assumed in order to relate k_{eddy} with k_L, while the model constant, β, was obtained by fitting the model with a large variation of highly accurate direct numerical simulations. It should be mentioned that for very small Stokes numbers the numerator of Eq. (20) might become negative. However, at these conditions no significant relative velocity between particles and fluid can exist. Therefore, if this is the case, we assume that $u_{rel} = 0$. This will result in a tiny discontinuities in the model prediction that will be visible in figures presented in Section 3.2.

By calculating the particle Reynolds number based on the relative velocity obtained from Eq. (20), the Ranz-Marshall model (see Eq. (6)) can now be used to find the *average* Sherwood number, $\overline{\mathrm{Sh}}$. As can be seen from Eqs. (19) and (20), the Sherwood number $\overline{\mathrm{Sh}}$ is affected by the turbulence only. The reaction rate due to diffusion given by Eq. (3) can now be modified to take into account the effect of turbulence and particle clustering as

$$R_{dif} = \tilde{\alpha} \frac{C}{d_p} \left(\frac{T + T_p}{2}\right)^{3/4}. \tag{24}$$

The model can therefore incorporate the effect of mean gas-particle velocity through Eqs. (5)–(7), as well as the effect of turbulence and particle clustering through Eqs. (9)–(15). As mentioned above, care should be taken when applying Eqs. (5)–(7) with the stochastic tracking method. It should also be stressed that Eqs. (9)–(15) are suitable to be applied in RANS models, and their form allows to determine all the required variables during the simulation. In this study, the model was implemented into ANSYS Fluent by means of a User Defined Function (UDF) mechanism. The UDF is provided as a supplementary file to this paper.

Table 1
The value of γ_{st} for some mixtures.

Mixture	Reaction	γ_{st}
Char particles in air	$C + O_2 \rightarrow CO_2$	11.4
Char particles in 100% CO_2	$C + CO_2 \rightarrow 2CO$	3.7
Char particles in 100% O_2	$C + O_2 \rightarrow CO_2$	2.7
Char particles in steam	$C + H_2O \rightarrow CO + H_2$	1.5
Ilmenite particles in air	$4FeTiO_3 + O_2 \rightarrow 4TiO_2 + 2Fe_2O_3$	0.225

3. Model sensitivity

In this section, numerical examples are presented in which the model applicability and the influence of the main model parameters is presented. The first two examples are just general calculations, while the last one is a simplified CFD simulation. This enables us to examine the potential conditions in which the effect of turbulence can be significant in practical systems.

3.1. Numerical example 1

Eq. (11) can be re-organized to yield the following expression for the integral time scale:

$$\tau_L = \frac{\rho_p d_p^2}{18 \rho \nu \mathrm{St}}. \tag{25}$$

The Damköhler number is then given as

$$\mathrm{Da} = \frac{\tau_L}{\tau_c} = \frac{\tau_L 2 D n_p A_p}{d_p} = \frac{\rho_p d_p^2 2 D n_p A_p}{18 \rho \nu \mathrm{St} d_p}, \tag{26}$$

where, for the considerations in this section, it has been assumed that $\overline{\mathrm{Sh}} = 2$. Furthermore, the solids density in the domain can be expressed as

$$\rho_s = \rho_g / \gamma_{st}, \tag{27}$$

where ρ_g is the gas density in the gas-solid mixture and γ_{st} is the stoichiometric air-fuel ratio. The value of γ_{st} for some mixtures is given in Table 1. Apart from char-based mixtures, ilmenite was also included due to its possible application since the ilmenite particles can serve as oxygen carriers in Chemical Looping Combustion. The particle number density can now be expressed as

$$n_p = \frac{6 \rho_g}{\pi d_p^3 \rho_p \gamma_{st}}. \tag{28}$$

The intrinsic density of the gas, ρ, is, however, almost the same as the gaseous density of the mixture, ρ_g, as long as the solid volume fraction is low. From the above, and by using that $A_p = \pi d_p^2$, it can be shown that

$$\mathrm{Da} = \frac{\rho_p d_p^2 12 D \rho_g \pi d_p^2}{18 \rho \nu \mathrm{St} \pi d_p^3 \rho_p \gamma_{st} d_p} = \frac{2 \rho_g}{3 \mathrm{Sc} \mathrm{St} \gamma_{st} \rho} \approx \frac{2}{3 \mathrm{Sc} \mathrm{St} \gamma_{st}}. \tag{29}$$

In Fig. 2, the Damköhler number, as calculated from Eq. (29), is shown as a function of Stokes number for the same cases as listed in Table 1. Clustering is expected to slow down the reactions for Damköhler numbers around or greater than unity [17]. From Fig. 2, it can be seen that for carbon oxidation in air the Damköhler number is larger than unity only for Stokes numbers smaller than 0.1.

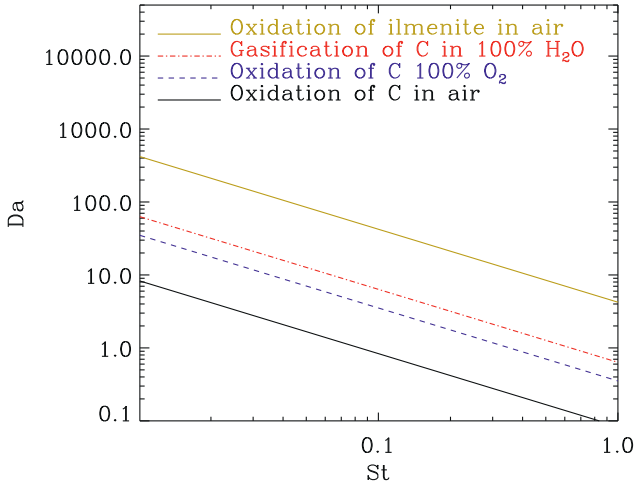

Fig. 2. Damköhler number at stoichiometric conditions as a function of Stokes number for the cases listed in Table 1. Here, the Schmidt number is set to Sc = 0.7.

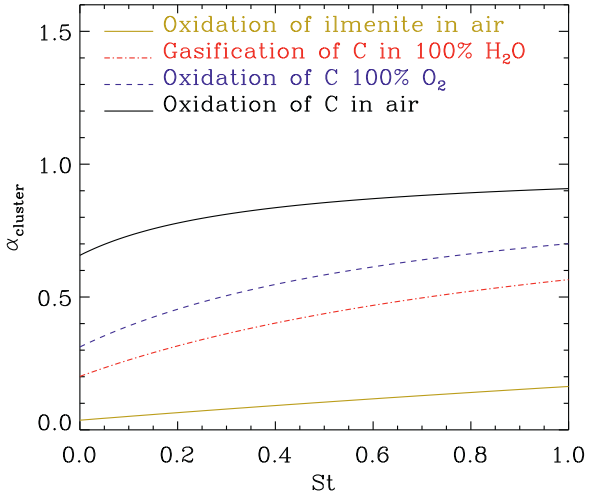

Fig. 3. Effect of clustering (α_{cluster}) as a function of Stokes number for the cases listed in Table 1.

For oxidation of ilmenite in air, however, the Damköhler number is above 4 even for Stokes number as large as one. Using Eqs. (10) and (29) the part due to clustering can be expressed as

$$\alpha_{\text{cluster}} = \frac{B}{B + \text{DaSt}/2} = \frac{0.08 + \text{St}/3}{0.08 + \text{St}/3 + 1/(3\text{Sc}\gamma_{st})}. \tag{30}$$

The value of α_{cluster} as a function of Stokes number is shown in Fig. 3, from which it is clear that the potential to reduce the reaction rate highly depends on the composition of the mixture. At stoichiometric conditions the reaction rate due to clustering can be reduced up to 35% in the case of char combustion in air, while for char combustion in pure O_2 or H_2O the effect of clustering can be twice as large. Finally, for oxidation of ilmenite in air, the reduction due to clustering is dramatic.

3.2. Numerical example 2

In this example we discuss the influence of selected model parameters on $\tilde{\alpha}$. The magnitudes of the studied parameters and other essential model parameters are presented in Table 2. They were selected such that they reflect, to some extent, conditions typically found in industrial scale facilities (reactors and combustion chambers). The required turbulence parameters, as would be known in a RANS simulation, were estimated.

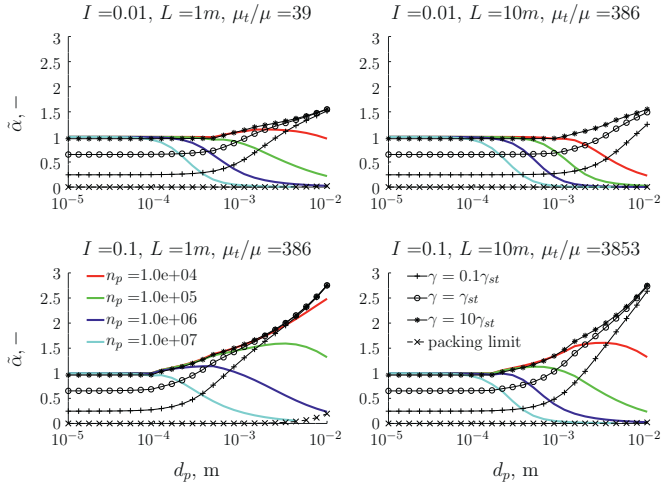

Fig. 4. The influence of parameters from Table 2 on $\tilde{\alpha}$ for char particles in air (ρ_p = 800 kg/m^3, γ_{st} = 11.4). The legend included in the bottom panels apply to the entire figure.

Table 2
Studied model input parameters.

Name	Symbol	Unit	Value
Mean gas velocity	u	m/s	10
Turbulence intensity	I	–	10^{-2}; 10^{-1}
Domain length scale	L	m	1; 10
Particle number density	n_p	m^{-3}	$10^4 - 10^7$
Gas density	ρ	kg/m^3	0.35
Gas kinematic viscosity	ν	m^2/s	10^{-4}
Diffusion coefficient	D	m^2/s	10^{-4}
Particle (material) density	ρ_p	kg/m^3	800

In order to calculate the turbulence kinetic energy k and its dissipation ε the following expressions were used

$$u_{rms} = uI, \tag{31}$$

$$k = \frac{3}{2}u_{rms}^2, \tag{32}$$

$$\varepsilon = C_\mu^{3/4}\frac{k^{3/2}}{l}, \tag{33}$$

where l is the integral length scale, approximated as $l = 0.07L$ [26], and $C_\mu = 0.09$ [27]. It should be noted that by using such a definition of l for large systems, the integral length scale is likely to be overestimated, which in turn leads to unrealistically high turbulent viscosity since

$$\mu_t = \rho C_\mu \frac{k^2}{\varepsilon} = \rho C_\mu^{1/4} k^{1/2} l. \tag{34}$$

Nevertheless, in the absence of problem-specific details, we stick to the above estimation.

The particle time scale τ_p, the time scale of the integral scale eddies τ_L and the chemical time scale τ_c are calculated from Eqs. (13)–(15), respectively. These time scales are then used to calculate St and Da, and the mean Sherwood number $\overline{\text{Sh}}$ is calculated using Eqs. (19)–(22) together with Eq. (6). The results, in the form of $\tilde{\alpha}(d_p)$ for selected particle number densities, are presented in Fig. 4 for the case of char particles in air. In the two upper panels, cases with low turbulence intensity ($I = 1\%$) are presented, whereas for the lower panels $I = 10\%$. Furthermore, the results shown in the left-hand side panels differ from those on the right side by the turbulence length scale, as stated in the title of the figure. There are four black lines in Fig. 4. The line with circle-shaped markers divides the figure into regions of rich (below the

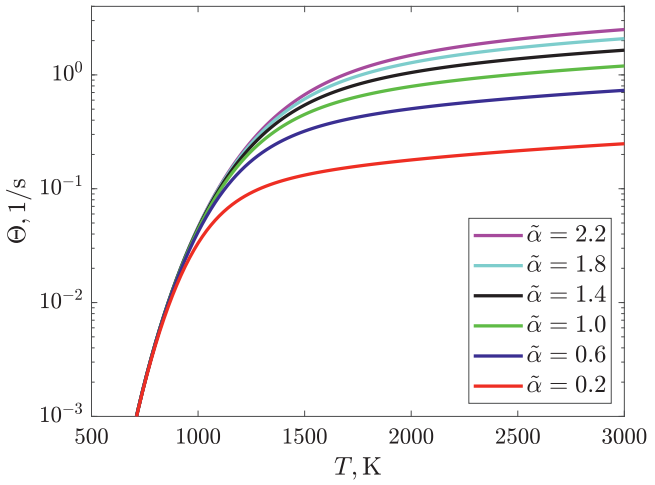

Fig. 5. The influence of $\tilde{\alpha}$ on the reactant consumption rate for $\rho_p = 800$ kg/m^3, $d_p = 500$ µm, $A = 0.002$ s/m, $E = 79$ kJ/mol, $C = 5 \cdot 10^{-12}$ sK$^{-3/4}$.

line) and lean (above the line) conditions, while the line with x-shaped markers corresponds to the packing limit of particles, i.e. the maximum volume fraction of the particles. For spherical particles, the volume fraction at the packing limit is assumed to be equal to 0.63, which is a typical limit for randomly packed, spherical particles of the same size. The remaining two lines encompass the region inside which the air-fuel ratio, γ, is between 0.1 and 10. It is expected that conditions in real systems correspond to the region limited by these two lines. Details regarding the derivation of the packing limit line and the stoichiometric line can be found in Appendix A.

From Fig. 4 it is clear that for the range of examined particle number densities, the turbulence do not have any effect on the mass transfer if the particles are too small. This is because particles for which $\tau_p << \tau_\eta$ immediately follow the motion of the fluid, so it is not possible for them to form clusters or for the turbulence to enhance the mass transfer due to any relative velocity between fluid and particle. (Please note that for d_p of the order of $10^{-5} - 10^{-4}$ Eq. (20) yields negative number inside the square root and in this region $u_{rel} = 0$ was assumed.) For larger particles, which have longer response times, both effects of turbulence can be observed. The largest mass transfer enhancement is, as expected, observed for the high turbulence intensity cases (lower panels of Fig. 4), in which $\tilde{\alpha}$ becomes greater than 1 if the particle number density is sufficiently low. For all cases above a certain n_p, the effect of particle clustering becomes dominant ($\tilde{\alpha} < 1$). This decrease in the reactant transfer rate is particularly strong for the low turbulence intensity cases (upper panels of Fig. 4) and it is more intense in larger facilities (right panels). It is also worth noticing that both scenarios are probable around the stoichiometric conditions, i.e. we can expect both effects of turbulence to be observed in real systems.

Finally, the influence of $\tilde{\alpha}$ on the reactant consumption rate Θ, as given by Eq. (2) in which R_{diff} is found from Eq. (24), is presented in Fig. 5 as a function of temperature. Resorting also to the results shown in Fig. 4, a factor of 2 enhancement of reaction rate due to turbulence ($\tilde{\alpha} > 1$) can be expected at favorable flow conditions and high temperatures. The reduction of the rate ($\tilde{\alpha} < 1$) can potentially be much stronger. In the following, we will investigate how $\tilde{\alpha}$ may vary in more realistic applications.

3.3. Numerical example 3

In order to visualize and quantify the effect of turbulence on pulverized char conversion, a simplified CFD model was developed.

Table 3
Stoichiometric coefficients for reaction (36) and volatiles composition.

$C_kH_lO_mN_nS_o$		ν_i	
k	1.034	O_2	1.258
l	2.682	CO	1.034
m	0.899	H_2O	1.341
n	0.0274	SO_2	0.0034
o	0.0034	N_2	0.0137

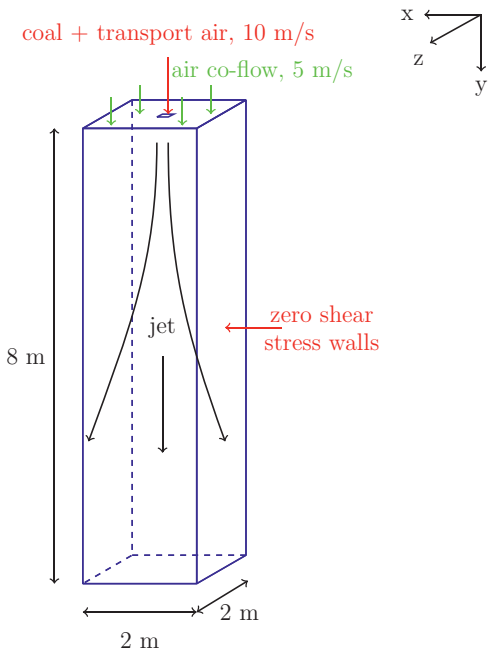

Fig. 6. Schematics of the geometry and boundary conditions.

The geometry of the model was selected to be a 2m × 2m × 8m cuboid to which coal particles are introduced through a square (4cm × 4cm) inlet together with a co-flowing hot air. Inside the domain the particles form a jet and undergo devolatilization and char combustion. The main features of the numerical approach are as follows. The Navier-Stokes equations are solved in a steady-state and incompressible form, turbulence is modelled using the standard $k-\varepsilon$ model, radiation is accounted for with the Discrete Ordinates model and the particles are tracked in a Lagrangian reference frame. For simplicity, and since the focus of the paper is on char conversion, the devolatilization rate is assumed constant (=50 1/s). A single surface reaction is considered:

$$C + O_2 \rightarrow CO_2 \tag{35}$$

where the corresponding Arrhenius parameters are $A = 0.002$ s/m, $E = 7.9 \cdot 10^7$ J/kmol and the diffusion constant from Eq. (3) is given by $C = 5 \cdot 10^{-12}$ s/K$^{-3/4}$, while the combustion rate of volatiles is computed using the Finite-Rate/Eddy-Dissipation model, according to the reaction:

$$C_kH_lO_mN_nS_o + \nu_{O_2}O_2 \rightarrow \nu_{CO}CO + \nu_{H_2O}H_2O + \nu_{SO_2}SO_2 + \nu_{N_2}N_2, \tag{36}$$

where the stoichiometric coefficients ν_i and the composition of the fictitious volatiles species $C_kH_lO_mN_nS_o$ are given in Table 3. A schematic representation of the geometry and boundary conditions are given in Fig. 6, coal properties are given in Table 4, and the main model parameters are presented in Table 5. The selection of this particular configuration was motivated by the fact that it reflects typical conditions for fuel supply to the combustion cham-

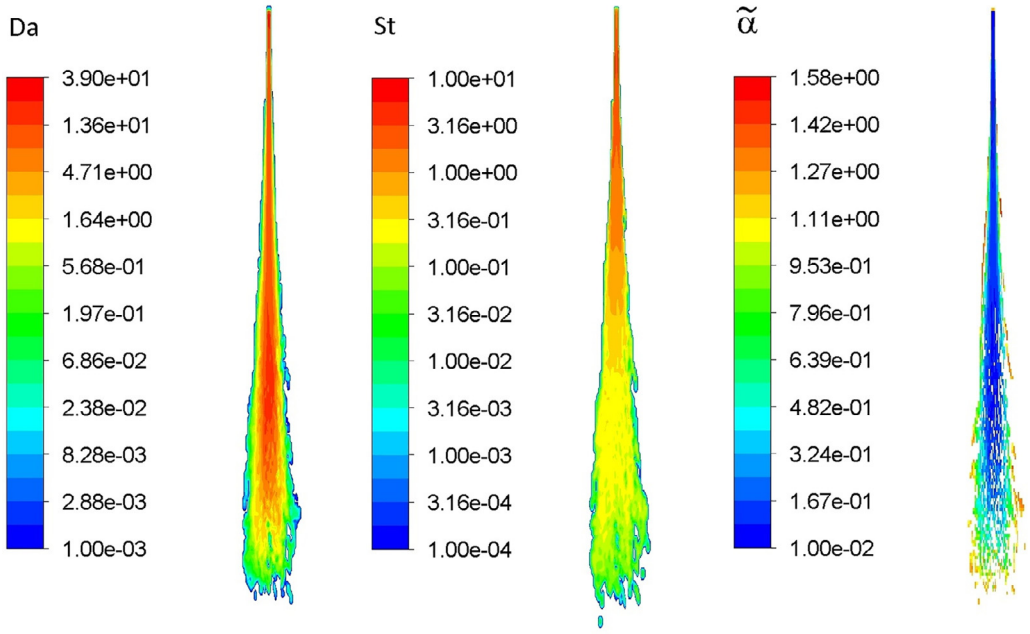

Fig. 7. Distribution of Da, St and $\tilde{\alpha}$ inside the jet.

Table 4
Coal properties.

Proximate analysis		Ultimate analysis (daf)	
Moisture	0.107	C	0.674
Volatiles	0.446	H	0.05
Fixed carbon	0.357	O	0.267
Ash	0.09	N	0.007
HCV (AR)	22.5 MJ/kg	S	0.002

Table 5
CFD model input parameters.

Name	Symbol	Unit	Value
Coal mass flow rate	m_f	kg/s	$1.5 \cdot 10^{-2}$
Transport air mass flow rate	$m_{air,1}$	kg/s	0.0056
Transport air temperature	$T_{air,1}$	K	1000
Coflow air mass flow rate	$m_{air,2}$	kg/s	7.0
Coflow air temperature	$T_{air,2}$	K	1000
Turbulence intensity	I	–	10^{-2}
Viscosity ratio	μ_t/μ	–	50
Coal (material) density	ρ_p	kg/m^3	1400
Coal particle diameter	d_p	m	$2.5 \cdot 10^{-4}$

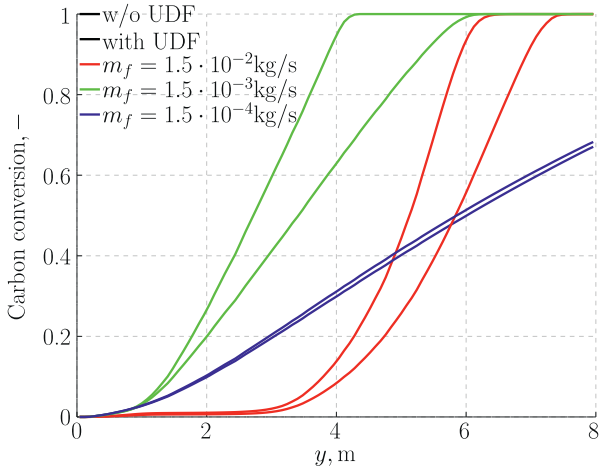

Fig. 8. Char conversion as a function of distance from the inlet - effect of fuel mass flow rate (in all cases $d_p = 2.5 \cdot 10^{-4}$ m).

ber. Moreover, the input parameters are chosen such that this set-up corresponds (to a certain degree) to the upper, left-hand side panel of Fig. 4, which means that the turbulence is most likely to reduce the mass transfer rate. The right panel of Fig. 7 shows the distribution of $\tilde{\alpha}$ in a cross section inside the jet. Please note that: 1) no interpolation (no smoothing between cell values) is used to produce contours of $\tilde{\alpha}$ in order to avoid a false impression of low $\tilde{\alpha}$ at the edges of the jet; 2) only regions with burning particles are displayed. From the figure it can be seen that, for the configuration considered, the effect of clustering is significant. In fact, $\tilde{\alpha}$ is of the order of 10^{-1} for the most part of the jet. An intensification in the mass transfer is predicted only at the edges of the jet, where the particle number density is lower and the turbulence intensity is highest. The reason the effect of turbulence is so strong can be understood by inspecting the Damköhler and Stokes numbers inside the jet. These two dimensionless numbers are shown in the left and middle panels of Fig. 7. Even though St decreases by 2–3 orders of magnitude along the particle jet, Da remains sufficiently high (of the order of 1) in the entire volume of the jet to yield $\tilde{\alpha} < 1$. It should also be noted that, based on Fig. 4, for $\tilde{\alpha}$ to decrease below 0.5 the local conditions must correspond to very rich mixture. For the case we study here, a relatively high fuel mass flow rate ($m_f = 1.5 \cdot 10^{-2}$ kg/s) was chosen to obtain such conditions but in reality the existence of large volumes with rich mixture is rather unlikely and mostly restricted to regions next to the fuel supply. Therefore, in the following we attempt to verify if the effect of turbulence still remains significant for lower fuel mass flow rates.

In Fig. 8 char conversion along the jet for three different fuel mass flow rates is presented. For each mass flow rate, two cases are shown. In the first, the baseline case, the effect of turbulence was not accounted for in the numerical model. In the second case, the effect of turbulence was introduced through the User Defined Function (UDF). This was done by modifying the reaction rate due to diffusion according to Eqs. (9), (10) and (24). In order to produce

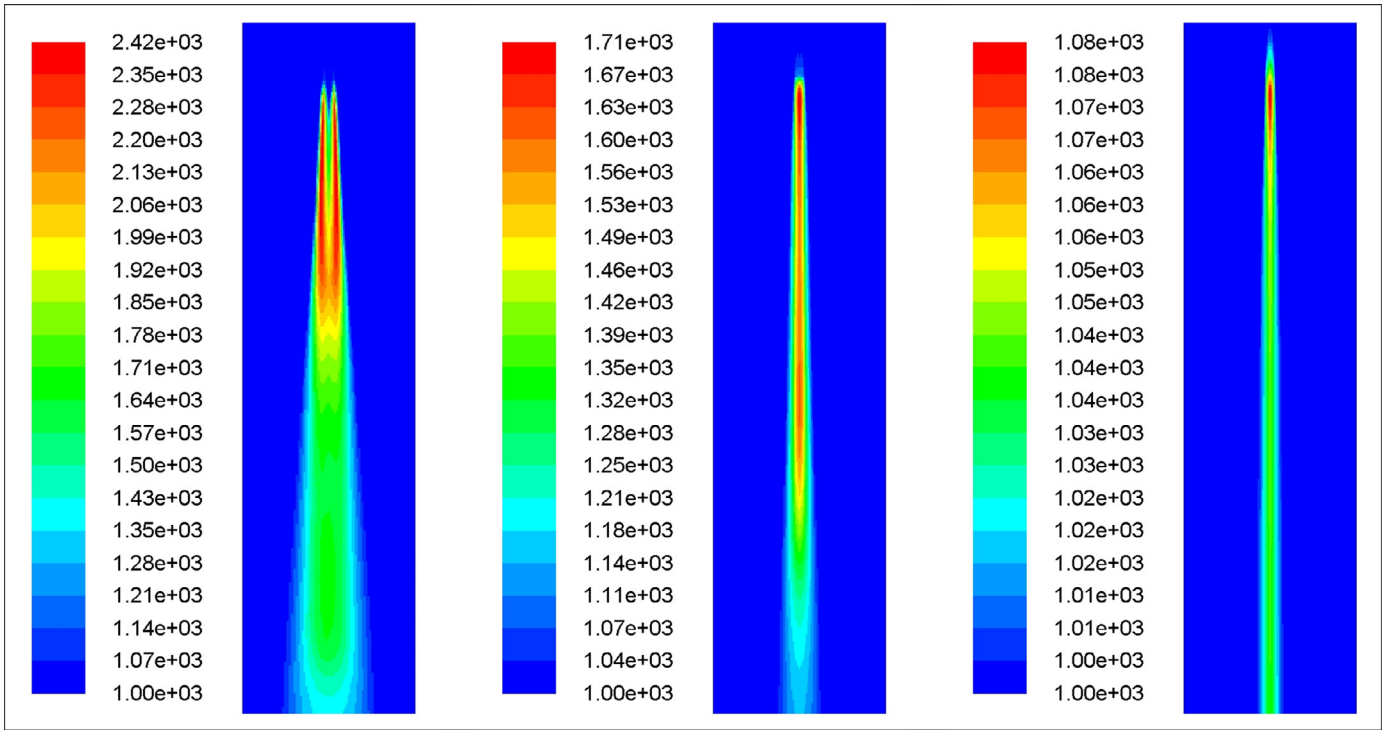

Fig. 9. Contours of temperature (in K) inside the particle jet, from left to right: $m_f = 1.5 \cdot 10^{-2}$ kg/s, $m_f = 1.5 \cdot 10^{-3}$ kg/s and $m_f = 1.5 \cdot 10^{-4}$ kg/s.

Fig. 8 the domain was divided into N segments along its height. For each such segment an average carbon conversion ($\overline{X}$) was computed for particles within the given section as

$$\overline{X} = \frac{1}{n_{part}} \sum_{i=1}^{n_{part}} X_i = \frac{1}{n_{part}} \sum_{i=1}^{n_{part}} \left(1 - \frac{m_c}{m_{c,0}}\right). \tag{37}$$

In the above, n_{part} is the number of particles passing through the given segment, m_c and $m_{c,0}$ are the current and initial particle char masses, respectively. The selected fuel mass flow rates can be thought of as rich ($m_f = 1.5 \cdot 10^{-2}$ kg/s), around-stoichiometric ($m_f = 1.5 \cdot 10^{-3}$ kg/s) and lean ($m_f = 1.5 \cdot 10^{-4}$ kg/s) mixtures, although we deliberately do not provide the exact magnitudes of air-fuel ratio (γ) as it varies significantly from cell to cell. It can be seen that turbulence has only a very weak positive effect on the conversion rate if the mass flow rate is very low or, in other words, if $\gamma >> \gamma_{st}$. The reason for that is a very low particle number density, and hence low Damköhler number. In regions with low Da, no dense clusters can be formed, so there is no reduction of the reaction rate due to clustering, but a weak increase due to turbulence ($\tilde{\alpha} > 1$). This behavior is also in agreement with the results presented in Fig. 4. In the cases with higher fuel mass flow rates in Fig. 8 (red and green lines), the particle number densities in the core of the jet are much higher, and a strong effect due to particle clustering can be observed as the conversion is much slower in the cases where the reaction rate is modified by the UDF. The conversion profiles are similar in both cases, but the conversion begins further downstream for the case with the highest mass flow rate.

It should be stressed that the results presented in Fig. 8 are strongly affected by the temperature. Even though the same boundary conditions were used, the cases with lower fuel mass flow rates are characterized by lower temperatures in the system due to the smaller amounts of released and burned volatiles. This is confirmed in Fig. 9, where the contours of temperature are presented. The consequence of higher temperature is higher reaction rate. This can be observed by comparing the slopes of the conversion profiles in Fig. 8, i.e. the higher the mass flow rate, the steeper the slope. At the same time, as the temperature increases, the diffusion rate becomes more important in the overall reaction rate, and thus the observed effect of turbulence is stronger. The difference in the reaction rates is more clearly visible in Fig. 10, which shows contours of the relative rate difference, defined as $(\Theta - \Theta_0)/\Theta_0$, where Θ is the modified rate including the effect of turbulence, and Θ_0 is the unmodified rate. The highest relative rate difference is observed for the highest mass flow rate, and it is smaller for the lower flow rate. It can be seen that the differences occur mostly in the core of the jet, where the particle number density, and hence the Damköhler number, are the highest, and thus the rate is considerably reduced. However, also regions of increased reaction rate are observed further away from the jet core. For the smallest mass flow rate the relative rate difference is not reduced in the center of the jet. Instead a slightly increased reaction rate can be observed at the jet outskirts, where the turbulence is strongest and the particle number density is quite low. Based on the results discussed above, we can conclude that the effect of particle clustering can be significant for a quite wide range of fuel mass flow rates or, in other words, for a wide range of stoichiometric conditions.

Another important parameter that influences how strong the effect of turbulence is, is the particle size. We examine this parameter by changing the particle diameter, but keeping the mass flow rate constant and equal to $1.5 \cdot 10^{-3}$ kg/s, corresponding to roughly stoichiometric conditions, for all cases. The particle sizes were chosen such that the particle number density n_p is decreasing by a factor of 10 as the particle diameter increases ($n_p \sim d_p^{-3}$). As can be seen in Fig. 11, for the smallest particles (red lines) the effect of turbulence amounts to essentially no difference when the total conversion is considered (i.e. the distance from the inlet to the point at which full conversion is reached). On the other hand, the local reduction of the conversion rate is actually of the same magnitude for all particle sizes. The reason the decreased reaction rate does not affect the total conversion time for the smallest particles is depletion of the available oxygen, seen as a flattening of the

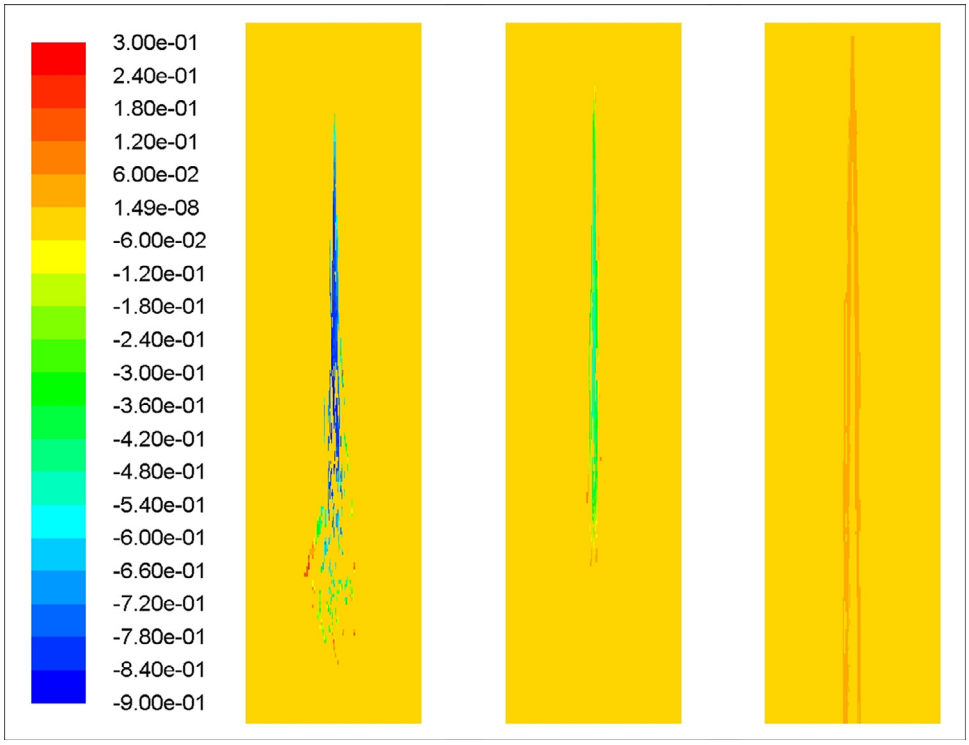

Fig. 10. Contours of relative rate differences $(\Theta - \Theta_0)/\Theta_0$ inside the particle jet, from left to right: $m_f = 1.5 \cdot 10^{-2}$ kg/s, $m_f = 1.5 \cdot 10^{-3}$ kg/s and $m_f = 1.5 \cdot 10^{-4}$ kg/s.

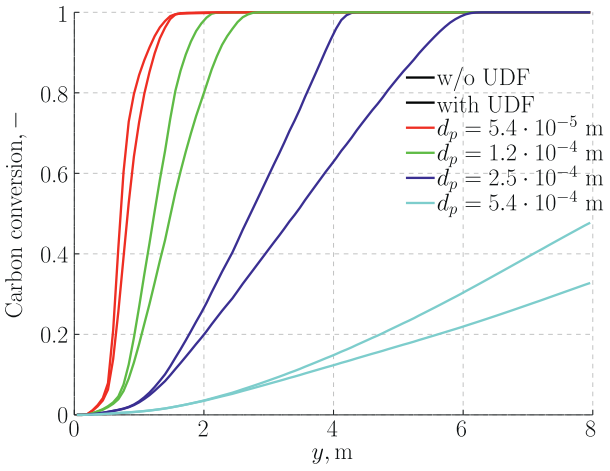

Fig. 11. Char conversion as a function of distance from the inlet – effect of particle diameter (in all cases $m_f = 1.5 \cdot 10^{-3}$ kg/s).

'without UDF' profile at the final stage of conversion. As the particle size becomes larger, particles travel further downstream before they reach a complete burnout. This is because these larger particles are less affected by fluid motions. Also, on average, they burn in lower temperatures as they still undergo conversion long after they have passed the regions of highest temperature, i.e. regions of volatile burning. For these larger particles, the effect of turbulence is more pronounced, e.g. particles with $d_p = 2.5 \cdot 10^{-4}$ m (dark blue lines) need to travel around 50% longer to reach complete burnout when the effect of turbulence is accounted for. This is opposite to what can be expected based on Fig. 4, since for a given stoichiometric condition $\tilde{\alpha}$ increases for larger particle sizes. Nevertheless, the degree to which the conversion rate is reduced depends not only on $\tilde{\alpha}$ but also on the relative magnitudes of R_{kin} and R_{dif}. As the particle diameter increases the conversion rate becomes more diffusion-controlled since $R_{dif} \sim 1/d_p$ (see Eq. (3)). At the same time, the rate due to kinetics varies only slightly. The resulting shift towards diffusion-controlled regime outweighs the effect of higher $\tilde{\alpha}$ and leads to the conversion rate being reduced by the same amount, irrespective of the particle size. Finally, it should be noted that for even larger particles, at some point $\tilde{\alpha} \geq 1$ (see Fig. 4), such that no reduction in the conversion rate due to clustering will be possible, even for a fully diffusion-controlled reaction. This was observed for particles with $d_p \sim 1 \cdot 10^{-3}$ m but was not shown in Fig. 11 due to much longer time scale required to reach even a fractional burnout.

The degree to which the turbulence influences the surface reaction rate might also depend on the characteristics of the turbulence itself, such as turbulence intensity or the viscosity ratio, μ_t/μ, as they are linked to turbulence kinetic energy and its dissipation. These two parameters can affect the integral time scale, and thus, the Damköhler and Stokes numbers. Their influence is shown in Fig. 12 from which it can be seen that the conversion rate is affected in almost exactly the same way for all parameter combinations that we study. The only difference is that a sufficiently strong turbulence causes the particles to be converted slightly faster as a result of enhanced mixing.

Finally, we observed that the effect of clustering weakens if the jet velocity (velocity at which the transport air and particles are introduced) is increased, as shown in Fig. 13. This is due to the Damköhler number being reduced as the jet velocity increases. At even higher jet velocity, the only effect of turbulence would be to increase the conversion rate as a result of enhanced mass transfer to the particle surface.

4. Application to an industrial scale boiler

In the previous section we explored potential conditions in which turbulence can enhance or decrease the surface reactions through the mass transfer rate. As shown by Haugen et al. [17] these conditions can be reduced to only two dimension-

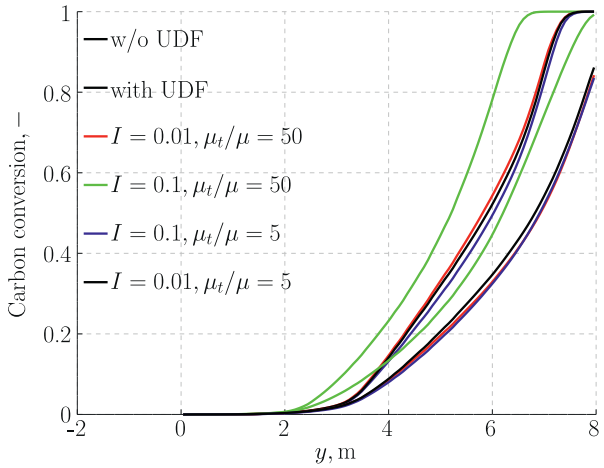

Fig. 12. Char conversion as a function of distance from the inlet – effect of inlet turbulence ($d_p = 2.5 \cdot 10^{-4}$ m, $m_f = 1.5 \cdot 10^{-2}$ kg/s, $T_{air} = 600$ K).

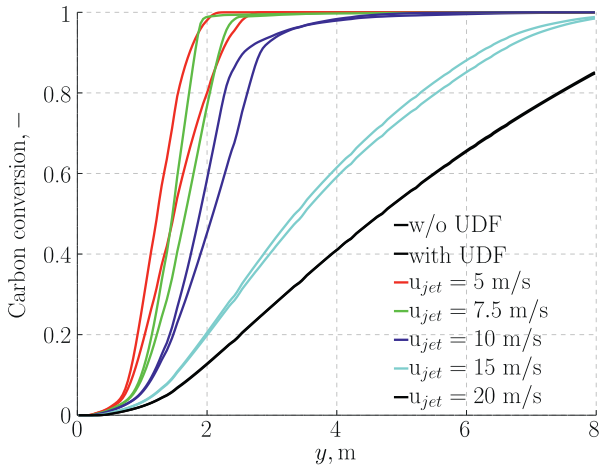

Fig. 13. Char conversion as a function of distance from the inlet – effect of jet inlet velocity ($d_p = 1.2 \cdot 10^{-4}$ m, $m_f = 1.5 \cdot 10^{-3}$ kg/s)

less numbers, the Stokes number and the Damköhler number. This implies that, in theory, one should be able to predict the effect of turbulence on the mass transfer rate in practical systems, such as large scale boilers, by a simple estimation of Da and St characterizing the given system. This is however not so straight forward since one has to deal with a certain range of these two parameters, often varying by several orders of magnitude. Thus, in order to verify how our theoretical considerations translate into reality, we examine a real-scale industrial boiler OP-430. This is a middle size boiler fired with a pulverized coal and producing 430 tones of steam per hour (at 532 °C, 12.7 MPa). Tangential firing is applied in the boiler, i.e. the burners are located in each of four corners of the furnace. A detailed description of the boiler geometry and operating conditions can be found in Adamczyk et al. [28]. A similar numerical approach to that described in Section 3.3 is utilized here, the main differences being: 1) lower devolatilization rate (=13 1/s), 2) slightly more accurate chemistry and 3) a different coal type. The considered reactions are:

$$C + \frac{1}{2}O_2 \rightarrow CO \tag{38}$$

$$CO + \frac{1}{2}O_2 + H_2O \rightarrow CO_2 + H_2O \tag{39}$$

Table 6
Stoichiometric coefficients for reaction (36) and volatiles composition.

$C_kH_lO_mN_nS_o$		ν_i	
k	1.19	O_2	1.54
l	4.41	CO	1.35
m	0.58	H_2O	2.17
n	0.068	SO_2	0.018
o	0.0027	N_2	0.040

Table 7
Coal properties.

Proximate analysis		Ultimate analysis (daf)	
Moisture	0.022	C	0.803
Volatiles	0.290	H	0.056
Fixed carbon	0.48	O	0.118
Ash	0.208	N	0.012
HCV (AR)	24.7 MJ/kg	S	0.011

Table 8
Kinetic parameters for reactions (38) and (39).

Reaction	A	E [J/kmol]	C [s/K$^{-3/4}$]
(38)	0.001	$7.9 \cdot 10^7$	$5 \cdot 10^{-12}$
(39)	$2.239 \cdot 10^{12}$	$1.7 \cdot 10^8$	–

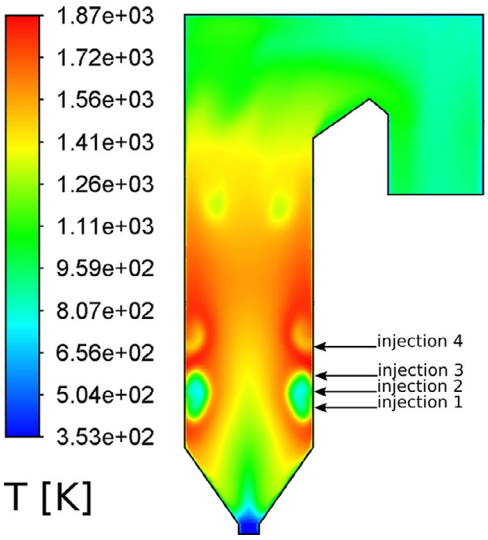

Fig. 14. Contours of temperature in the boiler central cross section. Arrows indicate elevations of fuel injection ports.

and the combustion of volatiles follow reaction (36) with the coefficients given in Table 6. The coal properties are listed in Table 7 and kinetic parameters given in Table 8.

In order to observe any effect of turbulence on the overall reaction rate it is required that the conditions inside the boiler correspond to zones II or III conversion. Otherwise, the conversion rate is fully limited by the reaction kinetics and the turbulence-affected mass transfer rate will have no influence on the process. Conditions in zones II and III are characterized by relatively high temperatures. Figure 14 shows the temperature distribution in the boiler central cross section. Four elevations at which coal is injected are also shown and marked with arrows. The pockets of low temperature located symmetrically close to the walls coincide with coal and air injections (pockets in the lower part) and overfire air ports (pockets in the upper part). The highest temperature can be observed around the particle injections and in the central part of the

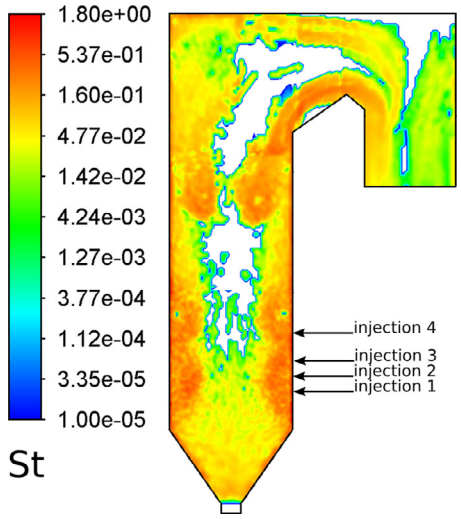

Fig. 15. Contours of the Stokes number. Arrows indicate elevations of fuel injection ports.

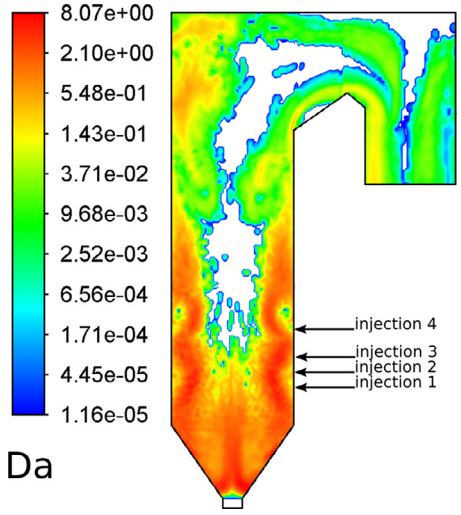

Fig. 16. Contours of the Damköhler number. Arrows indicate elevations of fuel injection ports.

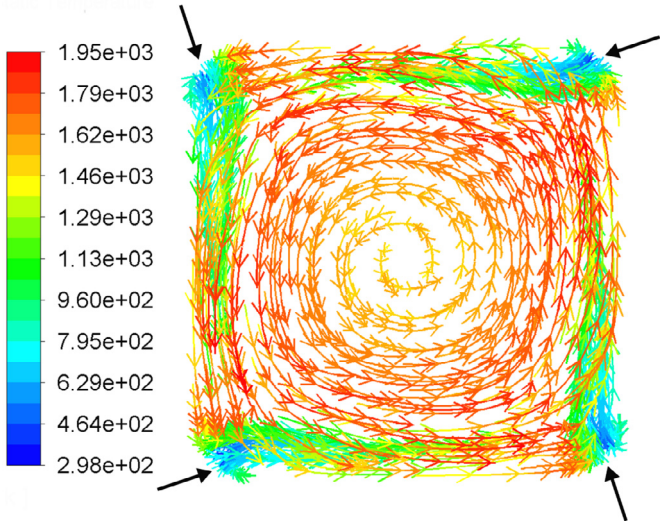

Fig. 17. Pathlines in the plane of injection 3 coloured by temperature [K]. Black arrows indicate locations and directions at which particles are introduced.

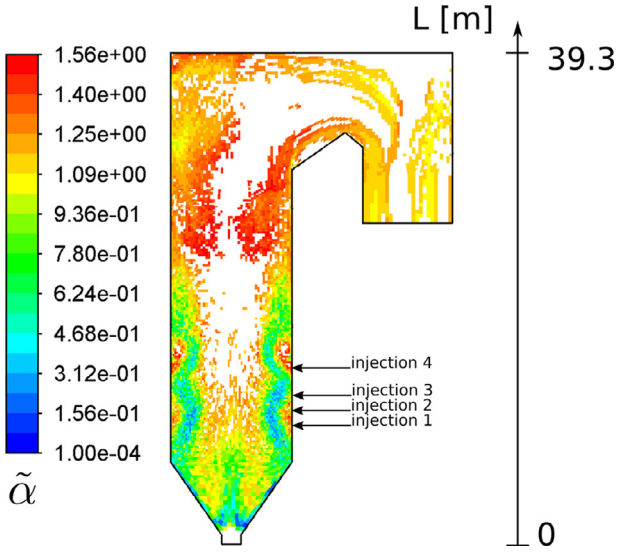

Fig. 18. Distribution of $\tilde{\alpha}$ in the boiler central cross section. Arrows indicate elevations of fuel injection ports.

boiler. These are the regions in which we can expect the conversion rate to be influenced by the turbulence.

The distribution of the Stokes and Damköhler numbers in the boiler cross section is shown in Figs. 15 and 16, respectively. In both figures, white zones in the central part correspond to regions in which there are no particles undergoing char combustion. The much higher density of particles in the vicinity of the boiler walls is caused by the specific design of injections, i.e. the particles are injected from the corners in a way that induces a spiraling motion (see Fig. 17, which shows pathlines in the injection area and locations at which the coal is injected). It can be seen that close to the walls in the lower part of the boiler both Da and St are relatively high. These conditions are favorable to particle clustering, thus, it is expected that the conversion process will slow down in these regions. This is in agreement with Fig. 18 which shows that $\tilde{\alpha}$ for these areas can be significantly less than one. On the other hand, in the upper part of the boiler, the Damköhler number is much lower. This is because of the particle number density, which is lower by around 2–3 orders of magnitude. In such regions the only effect turbulence can have is to intensify the reactant transport towards the particle surface, which is equivalent to saying that $\tilde{\alpha} > 1$, as can be seen in Fig. 18.

To investigate the effect of turbulence in this particular boiler, we compared the degree of carbon conversion along the boiler height in Fig. 19. These results were obtained in an equivalent way to Fig. 8. The four panels in the figure correspond to the four levels of particle injections as they are located at different heights in the boiler, as marked in Fig. 18. The points at which carbon conversion is lowest reveals where the particles are injected. Please note that the coal is introduced through all four injections simultaneously so the particles from different injections influence each other; it is only for clarity that we follow particles introduced through each injection separately and divide the results into four panels. It can be seen that for particles spiraling up the boiler the effect of turbulence on the conversion rate is rather insignificant, there is only a slight increase in the conversion rate for most injections, except for the injection 4 which is located the highest in the boiler. The situation changes for particles that travel down the boiler, i.e. the particles that are introduced mostly by injections 1 and 2. There, a clear reduction in the conversion rate can be observed which means that in these regions the conditions are just right for turbu-

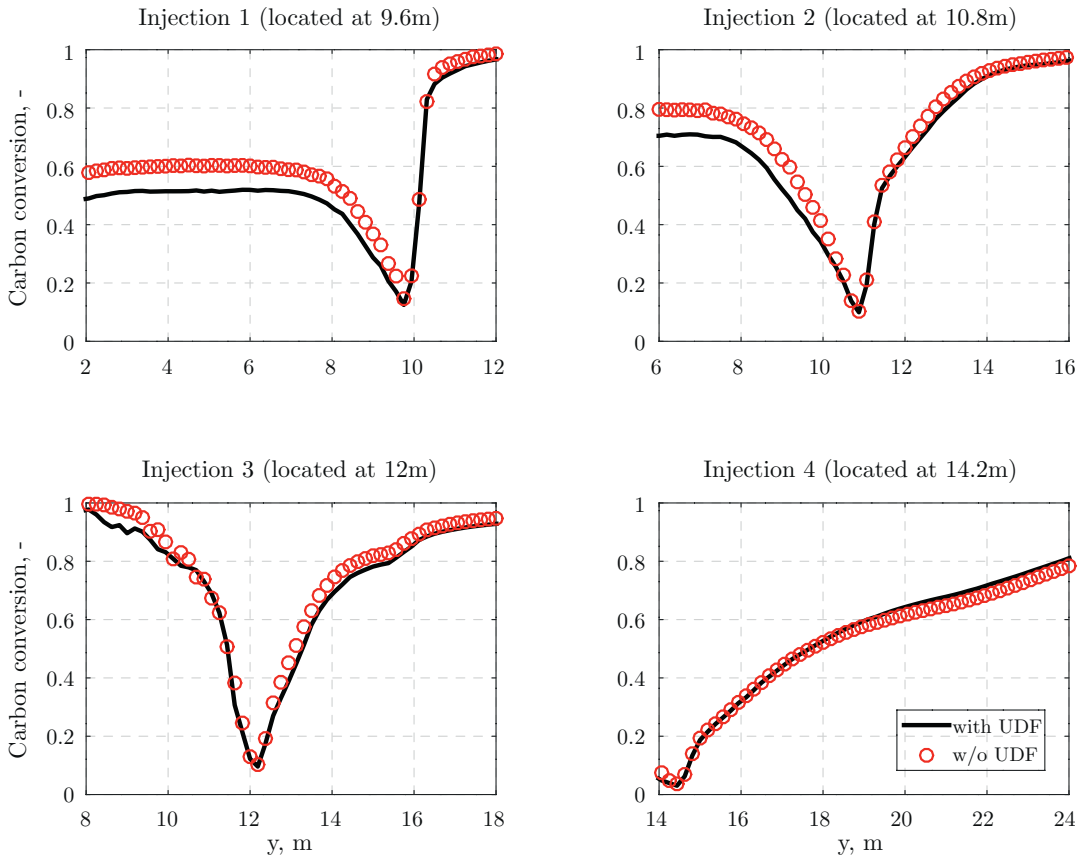

Fig. 19. Char conversion as a function of boiler height as predicted for the baseline case and the case with the UDF.

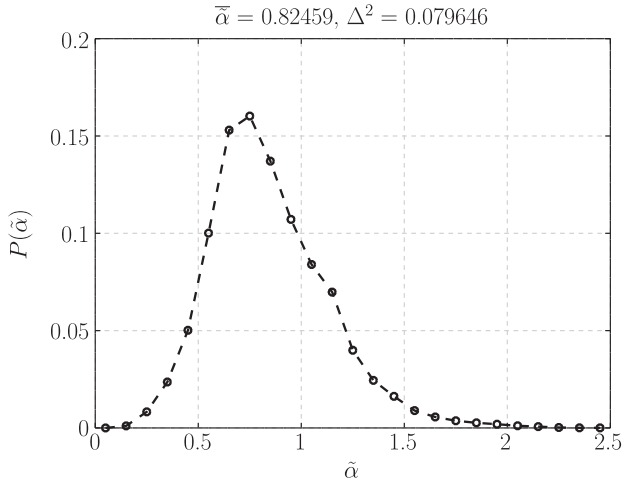

Fig. 20. Probability distribution of $\tilde{\alpha}$ inside the boiler.

lence to cause particle clustering. This is consistent with Fig. 18 in which $\tilde{\alpha}$ is smallest in the lower part of the boiler.

It should be noted that from Fig. 19 it is still not possible to deduce to what extent the overall conversion rate is affected and what fraction of particles has their conversion rate affected by clustering. This important information can be conveyed through Fig. 20, which presents probability distribution of $\tilde{\alpha}$ inside the boiler. From the figure, it can be seen that for majority (79.2%) of reacting particles $\tilde{\alpha} < 1$ and that on average $\tilde{\alpha} = 0.825$. Taking into account results in Fig. 18, it can be concluded that the particle concentration is much higher in the lower part of the boiler where $\tilde{\alpha} < 1$. However, despite the fact that such a large fraction of particles is affected by the effect of clustering, the global rate reduction given by

$$\text{Rate reduction} = 1 - \left(\sum_{i=1}^{n_{part}} \frac{m_{c,0,i}}{t_{c,i}}\right)_{\text{withUDF}} \Big/ \left(\sum_{i=1}^{n_{part}} \frac{m_{c,0,i}}{t_{c,i}}\right)_{\text{w/oUDF}} \tag{40}$$

is equal to 2.02% (in the above, t_c is a total combustion time). The reason that the global rate reduction is so low for this particular boiler, is that it is relatively cold in the volumes where $\tilde{\alpha}$ is small, which is typically in the bottom part of the boiler. This means that the conversion rate is largely controlled by kinetics in the same areas where the clustering happens to be slowing down the mass transfer. Hence, the effect of the slow mass transfer is diminished.

Overall, for this boiler, the influence of turbulence on the conversion rate is weaker than what could be anticipated based on our theoretical predictions. This highlights that many variables and the interplay between them are relevant when predicting the effect of turbulence on the char conversion rate. It also shows that it is difficult to determine a priori if this effect needs to be accounted for. Based on what we have learned from this study, we do believe that the effect of char clustering may have significantly more effect on other applications or boiler geometries.

5. Conclusions

It has recently been shown that turbulence may both increase and decrease the mass transfer rate to reacting pulverized particles. More specifically, turbulence may *decrease* the fluid-particle mass transfer rate when the life time of turbulence induced particle clusters is comparable to the consumption rate of any gaseous

reactant. If particle clustering is not important, the mass transfer rate to the particles may be *increased* due to turbulence induced relative velocity between particle and fluid. Both of these effects are accounted for in a natural manner if all relevant turbulent scales are resolved on the numerical mesh. This is the case for DNS and potentially also for well resolved large eddy simulations (LES), but it is *not* the case for RANS simulations. Naively, one may think that the classical turbulence particle dissipation model that is commonly used in many RANS simulations may accurately account for the relative velocity between particle and fluid. This is, however, not the case. Instead they are grossly overpredicting the relative velocity between particles and fluid and, hence, the mass transfer rate. This is particularly the case for smaller particles.

In the present work, we use the numerical model that was developed by Haugen et al. [17] to assess the effect of turbulence on the char conversion rate for two realistic cases. The first case is a simplified jet burner while the other is an industrial scale boiler. In addition, several theoretical examples are given to show the influence of the selected parameters. The most promising conditions to observe the effect of turbulence on the conversion rate were found to include relatively large particles, large-scale facilities, fuel-rich conditions, moderate turbulence intensity and a low stoichiometric air-fuel ratio.

From the simplified jet burner, we show that the effect of turbulence can be significant for a quite wide range of parameters, such as fuel mass flow rates, particle sizes and jet velocities. It is, however, crucial to consider how the selected parameters influence not only the mass transfer rate ($\tilde{\alpha}$), but also the ratio of the diffusion and kinetic rates. The reason for this is that for low temperatures, where the reactions are kinetically dominated, a reduction in the mass transfer rate will not have any effect on the conversion rate of char. Nevertheless, for some of the cases studied, the distance where full conversion of char was achieved was increased by 50% when proper account was made for the effect of turbulence.

The industrial scale boiler was studied as an example of a real practical system in which the turbulence can play a role. Inside the boiler, we did observe regions where the char conversion rate was both increased and decreased due to the turbulence. However, the density of particles in this kind of boiler is typically too low to observe a strong decrease in the global conversion rate of char. Similarly, the effect associated with relative velocity differences is rather minor. We expect this effect to show a greater importance in systems characterized by larger particles (higher Stokes numbers) since small particles quickly adjust to fluid motions without any significant relative velocity between them and the fluid.

Even though the effect of turbulence is not very dramatic in the industrial boiler studied here, we know from the example with the simplified burner that for certain conditions it will indeed have a strong effect. One should therefore always include the effect of turbulence in RANS simulations used for accurate predictions of char burnout.

In the future one should also study how turbulence affect the reaction rates of solid particles in other industrial facilities, such as char conversion in e.g. gasifiers or MILD combustors. Another interesting application would be oxidation of ilmenite in the air reactor of a Chemical Looping Combustion (CLC) system.

Declaration of Competing Interest

The authors declare that they have no known competing financial interests or personal relationships that could have appeared to influence the work reported in this paper.

Acknowledgments

The research leading to these results has received funding from the research projects: 'CHEERS', financed by the European Union's Horizon 2020 research and innovation program (grant agreement No. 764697), 'GASPRO', financed by the Research Council of Norway (grant agreement No. 267916) and Opus 13 operated by the Polish National Science Centre (project contract No. UMO-2017/25/B/ST8/00957). This study has been partially supported by the statutory research fund of the Silesian University of Technology, Faculty of Energy and Environmental Engineering, Institute of Thermal Technology, Gliwice, Poland.

Appendix A. Derivation of the stoichiometric number density $n_{p,st}$ and packing limit

The gas and solids volume fractions sum up to unity

$$\epsilon_s + \epsilon_g = \frac{V_s}{V} + \frac{V_g}{V} = 1 \tag{A.1}$$

$$\rho_s = \frac{m_s}{V} = n_p m_p = n_p \rho_p \frac{\pi d_p^3}{6} = \epsilon_s \rho_p \tag{A.2}$$

$$\rho_g = \frac{m_g}{V} = \rho \epsilon_g \tag{A.3}$$

$$\epsilon_s + \epsilon_g = \frac{\rho_s}{\rho_p} + \frac{\rho_g}{\rho} = 1 \tag{A.4}$$

$$\frac{1}{\rho_p} + \frac{\rho_g}{\rho_s \rho} = \frac{1}{\rho_s} \tag{A.5}$$

Taking the ratio of gas to solids such that it is stoichiometric

$$\gamma_{st} = \frac{\rho_g}{\rho_s} \tag{A.6}$$

and using Eqs. (A.2) and (A.5) becomes

$$\frac{1}{\rho_p} + \frac{\gamma_{st}}{\rho} = \frac{6}{n_{p,st} \rho_p \pi d_p^3} \tag{A.7}$$

$$n_{p,st} = \frac{6}{\rho_p \pi d_p^3} \frac{\rho \rho_p}{\gamma_{st} \rho_p + \rho} = \frac{6}{\pi d_p^3} \frac{1}{\gamma_{st} \frac{\rho_p}{\rho} + 1} \tag{A.8}$$

which for $\frac{\rho_p}{\rho} \gg 1$ becomes

$$n_{p,st} \approx \frac{6}{\pi d_p^3} \frac{\rho}{\gamma_{st} \rho_p} \tag{A.9}$$

For a given γ_{st}, $n_{p,st}$ is the stoichiometric particle number density, for which $\tilde{\alpha}$ can be determined. The relation between the particle number density n_p and solids volume fraction ϵ_s is

$$n_p = \frac{6}{\pi d_p^3} \epsilon_s. \tag{A.10}$$

Thus, for a given particle number density, the maximum diameter the particle can have without exceeding the packing limit can be computed from

$$d_{p,max} = \left(\frac{6 \epsilon_{s,max}}{\pi n_p} \right)^{1/3}. \tag{A.11}$$

The relation between the density ratio γ_{st} and solids volume fraction ϵ_s is

$$\epsilon_s = \frac{1}{\gamma_{st} \frac{\rho_p}{\rho} + 1} \tag{A.12}$$

From the above the solids volume fraction at stoichiometric conditions can be determined, i.e. for γ_{st} from Table 1.

Supplementary material

Supplementary material associated with this article can be found, in the online version, at doi:10.1016/j.combustflame.2020.12.040.

References

[1] H. Thunman, K. Davidsson, B. Leckner, Separation of drying and devolatilization during conversion of solid fuels, Combust. Flame 137 (1) (2004) 242–250, doi:10.1016/j.combustflame.2004.02.008.

[2] S. Saxena, Devolatilization and combustion characteristics of coal particles, Prog. Energy Combust. Sci. 16 (1) (1990) 55–94, doi:10.1016/0360-1285(90)90025-X.

[3] R.C. Borah, P. Ghosh, P.G. Rao, A review on devolatilization of coal in fluidized bed, Int. J. Energy Res. 35 (11) (2011) 929–963, doi:10.1002/er.1833.

[4] J. Yu, J.A. Lucas, T.F. Wall, Formation of the structure of chars during devolatilization of pulverized coal and its thermoproperties: a review, Prog. Energy Combust. Sci. 33 (2) (2007) 135–170, doi:10.1016/j.pecs.2006.07.003.

[5] M. Vascellari, R. Arora, M. Pollack, C. Hasse, Simulation of entrained flow gasification with advanced coal conversion submodels. Part 1: pyrolysis, Fuel 113 (2013) 654–669, doi:10.1016/j.fuel.2013.06.014.

[6] M. Vascellari, R. Arora, C. Hasse, Simulation of entrained flow gasification with advanced coal conversion submodels. Part 2: char conversion, Fuel 118 (2014) 369–384, doi:10.1016/j.fuel.2013.11.004.

[7] M. Baum, P. Street, Predicting the combustion behaviour of coal particles, Combust. Sci. Technol. 3 (5) (1971) 231–243, doi:10.1080/00102207108952290.

[8] M.A. Field, Rate of combustion of size-graded fractions of char from a low-rank coal between 1 200°K and 2 000°K, Combust. Flame 13 (3) (1969) 237–252, doi:10.1016/0010-2180(69)90002-9.

[9] R.H. Hurt, M.M. Lunden, E.G. Brehob, D.J. Maloney, Statistical kinetics for pulverized coal combustion, Symp. (Int.) Combust. 26 (2) (1996) 3169–3177, doi:10.1016/S0082-0784(96)80162-7.

[10] R. Hurt, J.-K. Sun, M. Lunden, A kinetic model of carbon burnout in pulverized coal combustion, Combust. Flame 113 (1) (1998) 181–197, doi:10.1016/S0010-2180(97)00240-X.

[11] S. Niksa, G.S. Liu, R.H. Hurt, Coal conversion submodels for design applications at elevated pressures. Part I. Devolatilization and char oxidation 29 (5) (2003) 425–477, doi:10.1016/S0360-1285(03)00033-9.

[12] G.S. Liu, S. Niksa, Coal conversion submodels for design applications at elevated pressures. Part II. Char gasification 30 (6) (2004) 679–717, doi:10.1016/j.pecs.2004.08.001.

[13] N.E.L. Haugen, M.B. Tilghman, R.E. Mitchell, The conversion mode of a porous carbon particle during oxidation and gasification, Combust. Flame 161 (2014) 612–619, doi:10.1016/j.combustflame.2013.09.012.

[14] N.E.L. Haugen, R.E. Mitchell, M.B. Tilghman, A comprehensive model for char particle conversion in environments containing O_2 and CO_2, Combust. Flame 162 (2015) 1455–1463, doi:10.1016/j.combustflame.2014.11.015.

[15] M.B. Tilghman, N.E.L. Haugen, R.E. Mitchell, A comprehensive char-particle gasification model adequate for entrained-flow and fluidized-bed gasifiers, Energy Fuels 31 (2015) 2164–2174, doi:10.1021/acs.energyfuels.6b02148.

[16] J. Krüger, N. Haugen, T. Løvås, D. Mitra, The effect of turbulence on the reaction rate of particles with heterogeneous surface reactions, Proc. Combust. Inst. 36 (2017) 2333–3240, doi:10.1016/j.proci.2016.06.187.

[17] N. Haugen, J. Krüger, D. Mitra, T. Løvås, The effect of turbulence on mass transfer rates of small inertial particles with surface reactions, J. Fluid Mech. 836 (2018) 932–951, doi:10.1017/jfm.2017.820.

[18] J. Krüger, N.E.L. Haugen, T. Løvås, Correlation effects between turbulence and the conversion rate of pulverized char particles, Combust. Flame 185 (2017) 160–172, doi:10.1016/j.combustflame.2017.07.008.

[19] E. Karchniwy, A. Klimanek, N. Haugen, The effect of turbulence on mass transfer rates between inertial polydisperse particles and fluid, J. Fluid Mech. 874 (2019) 1147–1168, doi:10.1017/jfm.2019.493.

[20] I. Smith, The combustion rates of coal chars: a review, Symp. (Int.) Combust. 19 (1) (1982) 1045–1065, doi:10.1016/S0082-0784(82)80281-6.

[21] D.D. Toporov, Combustion of Pulverised Coal in a Mixture of Oxygen and Recycled Flue Gas, Elsevier Insights, Elsevier, 2015, doi:10.1016/C2013-0-19301-4.

[22] A. Hayhurst, The mass transfer coefficient for oxygen reacting with a carbon particle in a fluidized or packed bed, Combust. Flame 121 (2000) 679–688, doi:10.1017/jfm.2017.820.

[23] L. Chen, S.Z. Yong, A.F. Ghoniem, Oxy-fuel combustion of pulverized coal: characterization, fundamentals, stabilization and CFD modeling, Prog. Energy Combust. Sci. 38 (2) (2012) 156–214, doi:10.1016/j.pecs.2011.09.003.

[24] W. Ranz, W. Marshall, Evaporation from drops, part I, Chem. Eng. Prog. 48 (3) (1952) 141–146.

[25] S. Kriebitzsch, A. Richter, LES simulation of char particle gasification at Reynolds numbers up to 1000, Combust. Flame 211 (2020) 185–194, doi:10.1016/j.combustflame.2019.08.028.

[26] W. Rodi, Turbulence Models and Their Application in Hydraulics – a State of the Art Review, NASA STI/Recon Technical Report A, 1980.

[27] B.E. Launder, D.B. Spalding, The numerical computation of turbulent flows, Comput. Methods Appl. Mech. Eng. (3) (1974) 269–289.

[28] W.P. Adamczyk, B. Isaac, J. Parra-Alvarez, S.T. Smith, D. Harris, J.N. Thornock, M. Zhou, P.J. Smith, R. Żmuda, Application of LES-CFD for predicting pulverized-coal working conditions after installation of NOx control system, Energy 160 (2) (2018) 693–709, doi:10.1016/j.energy.2018.07.031.